



#### **OPEN ACCESS**

EDITED BY

Adriaan Anthonius Lammertsma, University Medical Center Groningen, Netherlands

REVIEWED BY

Charalampos Tsoumpas, University Medical Center Groningen, Netherlands Klaus P. Schäfers, University of Münster, Germany

\*CORRESPONDENCE
Lorenzo Mercolli

I lorenzo,mercolli@insel.ch

RECEIVED 17 June 2025 ACCEPTED 17 October 2025 PUBLISHED 20 November 2025

#### CITATION

Mercolli L, Steinberger WM, Grundler PV, Moiseeva A, Braccini S, Conti M, Moskal P, Rathod N, Rominger A, Sari H, Schibli R, Seifert R, Shi K, Stepień EŁ and van der Meulen NP (2025) First positronium lifetime imaging with scandium-44 on a long axial field-of-view PET/CT.

Front. Nucl. Med. 5:1648621. doi: 10.3389/fnume.2025.1648621

#### COPYRIGHT

© 2025 Mercolli, Steinberger, Grundler, Moiseeva, Braccini, Conti, Moskal, Rathod, Rominger, Sari, Schibli, Seifert, Shi, Stepień and van der Meulen. This is an open-access article distributed under the terms of the Creative Commons Attribution License (CC BY). The use, distribution or reproduction in other forums is permitted, provided the original author(s) and the copyright owner(s) are credited and that the original publication in this journal is cited, in accordance with accepted academic practice. No use, distribution or reproduction is permitted which does not comply with these terms.

# First positronium lifetime imaging with scandium-44 on a long axial field-of-view PET/CT

Lorenzo Mercolli<sup>1,2,3</sup>\*, William M. Steinberger<sup>4</sup>, Pascal V. Grundler<sup>5</sup>, Anzhelika Moiseeva<sup>5</sup>, Saverio Braccini<sup>3</sup>, Maurizio Conti<sup>4</sup>, Paweł Moskal<sup>6,7</sup>, Narendra Rathod<sup>1,2</sup>, Axel Rominger<sup>1</sup>, Hasan Sari<sup>1,2,8</sup>, Roger Schibli<sup>5,9</sup>, Robert Seifert<sup>1,2</sup>, Kuangyu Shi<sup>1,2</sup>, Ewa Ł. Stepień<sup>6,7</sup> and Nicholas P. van der Meulen<sup>5,10</sup>

<sup>1</sup>Department of Nuclear Medicine, Inselspital, Bern University Hospital, University of Bern, Bern, Switzerland, <sup>2</sup>ARTORG Center for Biomedical Engineering Research, University of Bern, Bern, Switzerland, <sup>3</sup>Albert Einstein Center for Fundamental Physics (AEC), Laboratory for High Energy Physics (LHEP), University of Bern, Bern, Switzerland, <sup>4</sup>Siemens Medical Solutions USA, Inc., Knoxville, TN, United States, <sup>5</sup>Center for Radiopharmaceutical Sciences, PSI Center for Life Sciences, Villigen-PSI, Switzerland, <sup>6</sup>Faculty of Physics, Astronomy and Applied Computer Science, Jagiellonian University, Krakow, Poland, <sup>7</sup>Centre for Theranostics, Jagiellonian University, Krakow, Poland, <sup>8</sup>Siemens Healthineers International AG, Zürich, Switzerland, <sup>9</sup>Department of Chemistry and Applied Biosciences, ETH Zurich, Zurich, Switzerland, <sup>10</sup>Laboratory of Radiochemistry, PSI Center for Nuclear Engineering and Sciences, Villigen-PSI, Switzerland

**Purpose:** The physical properties of <sup>44</sup>Sc, combined with its imminent clinical application, position it as a prime candidate for *in vivo* positronium lifetime imaging. In this study, we investigate the count statistics for orthopositronium (oPs) measurements with <sup>44</sup>Sc on a commercial long-axial field-of-view (LAFOV) PET/CT.

**Method:** A NEMA image quality phantom was filled with 41.7 MBq of  $^{44}$ Sc dissolved in water and scanned on a LAFOV PET/CT. Three-photon events were identified using a prototype feature of the scanner and dedicated software. The lifetime of oPs was determined in the phantom spheres and in  $4 \times 4 \times 4$  mm<sup>3</sup> voxels.

**Results:** All measured oPs lifetimes are compatible, within the uncertainties, with the literature values for water. The oPs lifetime is  $2.65 \pm 0.50$ ,  $1.39 \pm 0.20$  and  $1.76 \pm 0.18$  ns in the three smallest spheres of the phantom and  $1.79 \pm 0.57$  ns for a single voxel in the central region of the largest sphere. The relative standard deviation in the background regions of the time difference distributions, i.e., for time differences smaller than -2.7 ns, is above 20%—even for voxels inside the phantom spheres.

**Conclusions:** Despite the favorable physical properties of <sup>44</sup>Sc, the count statistics of three-photon events remains a challenge. The high prompt-photon energy causes a significant amount of random three-photon coincidences with the given methodology and, therefore, increases the statistical uncertainties on the measured oPs lifetime.

#### KEYWORDS

scandium-44, long axial field-of-view PET/CT, positronium, positronium lifetime imaging, NEMA phantom

### 1 Introduction

Investigating the lifetime of ortho-positronium (oPs), the spin-1 state of an electron-positron bound system, has offered valuable insights into the structural properties of matter for decades (1-8). More recently, the medical community has shown interest in measuring oPs lifetimes in human tissue (9-12). So-called oPs lifetime imaging, i.e., constructing a threedimensional image of the human body with the oPs lifetime as voxel value (13), has the potential to provide diagnostic information about the tissue microenvironment, in particular oxygenation levels, that is currently unavailable in clinical routine (13-23). Recently, the first in vivo oPs lifetime images were determined with the dedicated multi-photon J-PET scanner prototype (24), and notably also the first in vivo oPs lifetime measurements with a commercial PET/CT system were demonstrated (25, 26). Different dedicated image reconstruction techniques for oPs lifetime imaging have been presented in the literature (20, 22, 27-32).

The oPs lifetime can be measured by determining the time difference between a prompt-photon, emitted during the nuclear decay along with the positron, and the two photons with 511 keV energy from the positron annihilation. The promptphoton serves as the start time, while the detection of the annihilation photons sets the stop time. The two annihilation photons are also used to determine the place of annihilation (33). Histograming all measured time differences gives a Positron Annihilation Lifetime (PAL) spectrum that contains several components, including the oPs lifetime. The oPs lifetime is of particular interest, as it depends on the molecular structure of the surrounding matter (9, 10). oPs lifetime measurements require a positron-emitting radionuclide with prompt-photon emission, together with the possibility of detecting and localizing three-photon events  $(3\gamma E)$ . The detection of  $3\gamma E$ poses significant challenges, particularly in a clinical environment. Positron emission tomography (PET) systems are designed to detect photon pairs with 511 keV energy. The detection of single-photon events with different energies is not part of the core design of clinical PET/CT scanners. Nonetheless, Ref. (34) presented the first use of a clinical PET/ CT scanner for oPs lifetime measurements by extending the detection and processing capabilities to 3yE. An accurate measurement of oPs lifetime requires the detection of a substantial number of  $3\gamma E$ . The increased sensitivity of longaxial field-of-view (LAFOV) PET/CT systems (35-38) proved to be a key factor for oPs lifetime measurement on a commercial PET/CT system.

Radionuclides with prompt-photon emission are readily available in clinics, of which <sup>68</sup>Ga labeled with [<sup>68</sup>Ga]Ga-PSMA-617 and [<sup>68</sup>Ga]Ga-DOTA-TOC is by far the most

<sup>1</sup>In this study, we do not consider three-photon decays of oPs.

widely adapted. <sup>82</sup>Rb and to some extent <sup>124</sup>I are also used in clinical routine, which is why Refs. (24, 25) relied on <sup>68</sup>Ga and <sup>82</sup>Rb for *in vivo* measurements. The prompt-photon branching ratio (BR $_{\gamma}$ ) is, of course, a key physical parameter to maximize the count statistics of  $3\gamma$ E. <sup>68</sup>Ga and <sup>82</sup>Rb have only a limited BR $_{\gamma}$ . If the positron emission fraction is taken into account, also the seemingly high BR $_{\gamma}$  of <sup>124</sup>I drops significantly. <sup>44</sup>Sc, on the other hand, has a very high BR $_{\gamma}$  in conjunction with a high positron fraction, which makes it a prime candidate for oPs lifetime imaging (38, 39). There is legitimate hope that <sup>44</sup>Sc can overcome the challenge of detecting enough  $3\gamma$ E for a reliable determination of the useful lifetime of oPs (38).

Although  $^{44}\text{Sc}$  is not yet available in clinical routine, production routes, purification and labeling as well as first inhuman studies have been reported in the literature (40–49).  $^{44}\text{Sc}$  can be paired with its therapeutic analog  $^{47}\text{Sc}$  for theranostic applications, enabling seamless transitions between diagnostic imaging and targeted therapy. Adding diagnostic information from oPs lifetime imaging could boost the tailored effectiveness of therapeutic applications with  $^{47}\text{Sc}$ , the  $\beta^-$ -emitting theranostic partner of  $^{44}\text{Sc}$ .

In this brief report, we investigate the properties of  $^{44}$ Sc for oPs lifetime imaging on a commercial LAFOV PET/CT. While Refs. (25, 34, 50) showed that  $^{124}$ I outperforms  $^{68}$ Ga and  $^{82}$ Rb in terms of  $^{3}\gamma$ E count statistics, the current study investigates the performance of  $^{44}$ Sc with respect to oPs lifetime imaging and how it compares to  $^{124}$ I using the methodology described in Refs. (25, 34, 50).

#### 2 Method

44Sc was produced at the Paul Scherrer Institute (PSI, Switzerland). The radionuclide production and post-irradiation processing at PSI have been established and are being further developed and optimized, as documented in Refs. (46, 51, 52). At Inselspital's Department of Nuclear Medicine (Switzerland) a standard NEMA image quality phantom (Data Spectrum Corp.) without lung insert was filled with a total of 41.7 MBq at scan time. The dose calibrator in the Department of Nuclear Medicine (VDC-405/VIK-202, Comecer, The Netherlands) was cross-calibrated with a 44Sc reference activity from PSI. Ref. (53) describes the calibration of PSI's dose calibrator for 44Sc. The activity concentration in the six phantom spheres at scan time was 40.68 kBq/mL while the background concentration was 3.90 kBq/mL. The phantom was scanned for 20 min in the socalled singles mode on a Biograph Vision Quadra (Siemens Healthineers, USA). Singles mode stores all single-crystal interactions into a list mode file. The sorting of  $3\gamma E$  is performed using the same prototype software as described in Refs. (25, 34, 50). The annihilation photon energy window is 476 to 546 keV with a double coincidence time window of 4.2 ns, while the prompt-photon energy window is 720 to 735 keV, i.e., the last two energy bins. Apart from the time and energy window selection, a minimal distance of 30 crystals

(equivalent to a 100 mm radius) is applied in order to control the  $^{176}$ Lu background (34). No reconstruction algorithm is applied, i.e., the spatial localization of the  $3\gamma E$  is purely based on time-of-flight (TOF) of the 511 keV photons (34). As described in Ref. (34), Quadra resolves photon energies up to 726 keV. Beyond this energy, all detected photons are collected in a single energy bin. Since the prompt-photon of  $^{44}$ Sc has an energy of  $1157.022 \pm 0.015$  keV, all prompt-photon events are located in the last energy bin. The time differences between the annihilation and prompt-photons for each  $3\gamma E$  were binned in order to obtain a PAL spectrum. The time bins are 133 ps wide. For the parameter fit we select only those  $3\gamma E$  with time differences between -2 ns and 8.6 ns.

For the determination of the oPs lifetime, we rely on the same Bayesian fitting procedure as in Refs. (25, 34, 50). The fit model for the PAL spectrum consists of three lifetime components, i.e., direct annihilation, para-positronium and oPs, convoluted with a Gaussian function that models the detection system. Solving the convolution integral analytically, the fit model can be written in terms of error functions:

$$F(\Delta t) = b + N \cdot \sum_{c=1}^{3} \frac{BR_c}{2\tau_c} e^{(\sigma^2 - 2\Delta t \, \tau_c + 2\Delta_0 \, \tau_c)/(2\tau_c^2)}$$

$$\cdot \operatorname{erfc}\left(\frac{\sigma}{\sqrt{2}\tau_c} + \frac{\Delta_0 - \Delta t}{\sqrt{2}\sigma}\right). \tag{1}$$

In Equation 1, b denotes a constant background and N is a normalization constant. The relative branching ratios of the three lifetimes  $\tau_{1,2,3}$  are  $BR_{1,2,3}$ . The two parameters  $\sigma$  and  $\Delta_0$  define the Gaussian function. They represent the timing resolution and time offset. We use a Bayesian fitting procedure that minimizes a Gaussian likelihood for determining the parameter's posterior distributions. Equation 2 shows the prior distributions for the fit parameters

$$au_3 \sim \mathcal{N}(1.78 \text{ ns}, 0.8 \text{ ns}), \ BR_{1,2,3} \sim \text{Dirichlet}(0.75, 3.1, 1.15), \ \sigma \sim \mathcal{N}(0.1 \text{ ns}, 0.05 \text{ ns}), \ \Delta \sim \mathcal{N}(0 \text{ ns}, 0.5 \text{ ns}), \ N \sim \mathcal{N}(A, 0.1 \cdot A), \$$
 (2)

where A is the integrated of the PAL spectrum with a subtracted background b. The value of b is determined as the mean counts with time differences smaller than  $-2.7\,\mathrm{ns}$ . The values of the direct annihilation and oPs lifetime are fixed to reference values of  $\tau_1 = 0.388\,\mathrm{ns}$  and  $\tau_2 = 0.125\,\mathrm{ns}$ . Setting priors for  $\tau_{1,2}$  does not impact the result significantly (25, 34). The Bayesian approach allows us to marginalize nuisance parameters. In fact, we are mostly interested in  $\tau_3$  and the branching ratios (for sanity checks and comparison with established results from the literature). We report the fit results in terms of marginalized posterior distributions. The posterior distribution for  $\tau_3$  is almost a perfect Gaussian function, hence the standard deviation is a reasonable measure for the uncertainty. However, this does

not apply to  $BR_{1,2,3}$  and we therefore provide the highest density interval (HDI) of the posterior distribution in the results.

We determined the oPs lifetime for the six spheres  $s_{1\cdots 6}$  of the NEMA phantom (nominal diameters: 10, 13, 17, 22, 28, 37 mm). Furthermore, we binned the spatial distribution of the detected  $3\gamma E$  into voxels of  $4\times 4\times 4$  mm<sup>3</sup>. For each voxel, the oPs lifetime is determined according to the same Bayesian fitting as for the phantom spheres.

# 3 Results

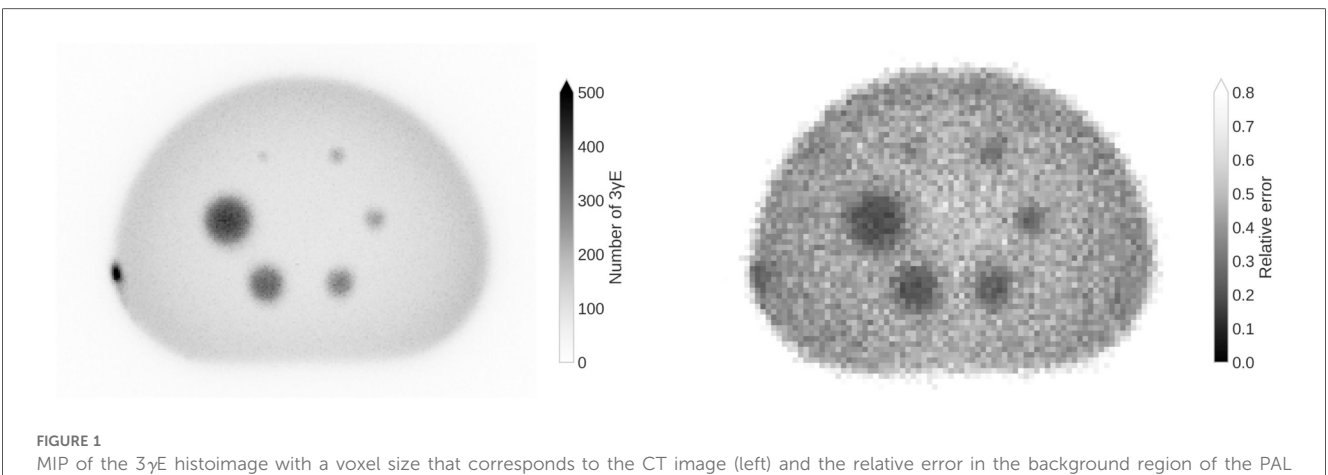
The left panel of Figure 1 shows the maximum intensity projection (MIP) of the  $3\gamma E$  histoimage. The binning is chosen according to the CT image, i.e.,  $1.52 \times 1.52 \times 1.65 \,\mathrm{mm^3}$ . Even without any reconstruction methodology, i.e., using only TOF for the localization of the  $3\gamma E$ , the smallest sphere  $s_1$  of the NEMA phantom is visible. The absence attenuation correction is clearly visible through the darkening on the border of the phantom. Some  $^{44}$ Sc activity stuck to the left wall of the phantom.

The total number of  $3\gamma E$  in the full field of view collected during the 30 min scan is  $539\,862\,149$  for a triple coincidence time window from  $-15\,\mathrm{ns}$  to  $+15\,\mathrm{ns}$ . These are, however, mostly random  $3\gamma E$ . In contrast, a 20 min scan in standard coincidence mode with a larger coincidence window of  $435\,\mathrm{keV}$  to  $585\,\mathrm{keV}$  of the same phantom yields  $2\,405\,451\,960$  net trues. This includes the standard random correction methods for coincidence PET.

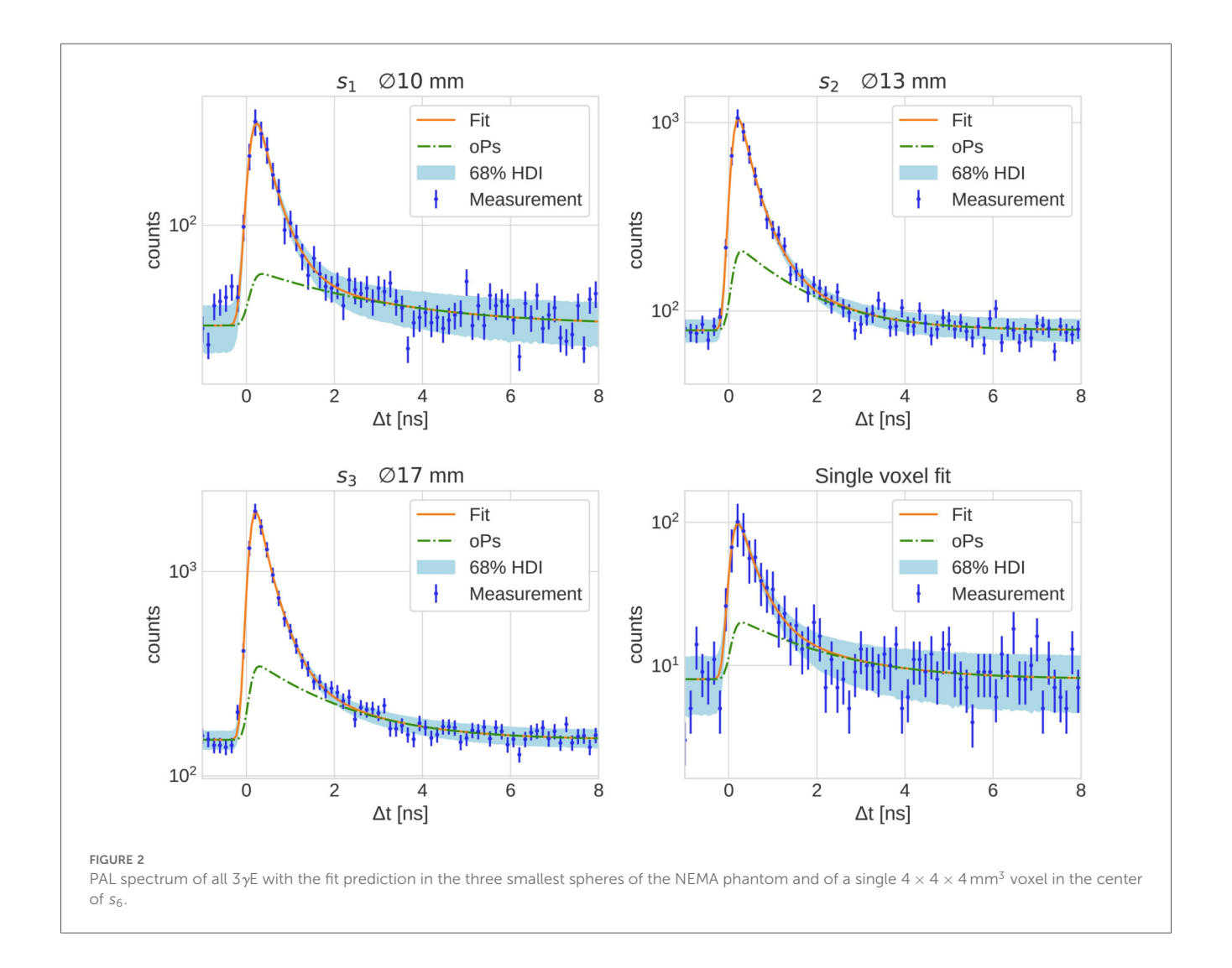
On the right of Figure 1 the relative error in the background region of the PAL spectrum, i.e., for time differences that are smaller than  $-2.7\,\mathrm{ns}$ , is shown. The error inside the spheres decreases as there is a higher activity concentration. Due to the decreasing number of  $3\gamma\mathrm{E}$  towards the center of the phantom, the error increases towards the center of the phantom (there is no attenuation correction).

Figure 2 shows the measured PAL spectrum with the fit prediction for the three smallest spheres and a single voxel in the center of the largest sphere  $s_6$ . The error bars plotted on the measurement points are the relative error in the background region of the PAL spectrum, i.e., the relative standard deviation of all time differences < -2.7 ns. The 68% HDI plotted in Figure 2 represents prediction uncertainty of the fit. The fit results corresponding to the PAL spectrum in Figure 2 are reported in Table 1 together with the fit results of the larger phantom spheres. The posterior distribution of  $\tau_3$  is Gaussian, hence we report the error on  $\tau_3$  as a standard deviation in Table 1. This does not apply to the relative branching ratios of the three lifetime components  $BR_{1,2,3}$ , since these are Dirichlet distributed random variables. Their error is therefore quoted as a 68% HDI.

In Figure 3 a slice of the full oPs lifetime image, together with the fit error on  $\tau_3$  with a  $4 \times 4 \times 4 \,\mathrm{mm}^3$  binning, is presented. While the oPs lifetime image is not particularly interesting -after all, the phantom is filled with water - the marginalized uncertainty on  $\tau_3$  clearly increases in the central region of the phantom. Note that only for the four largest spheres, the error decreases visibly.



spectrum in a single slice with  $4 \times 4 \times 4 \text{ mm}^3$  voxel size (right).



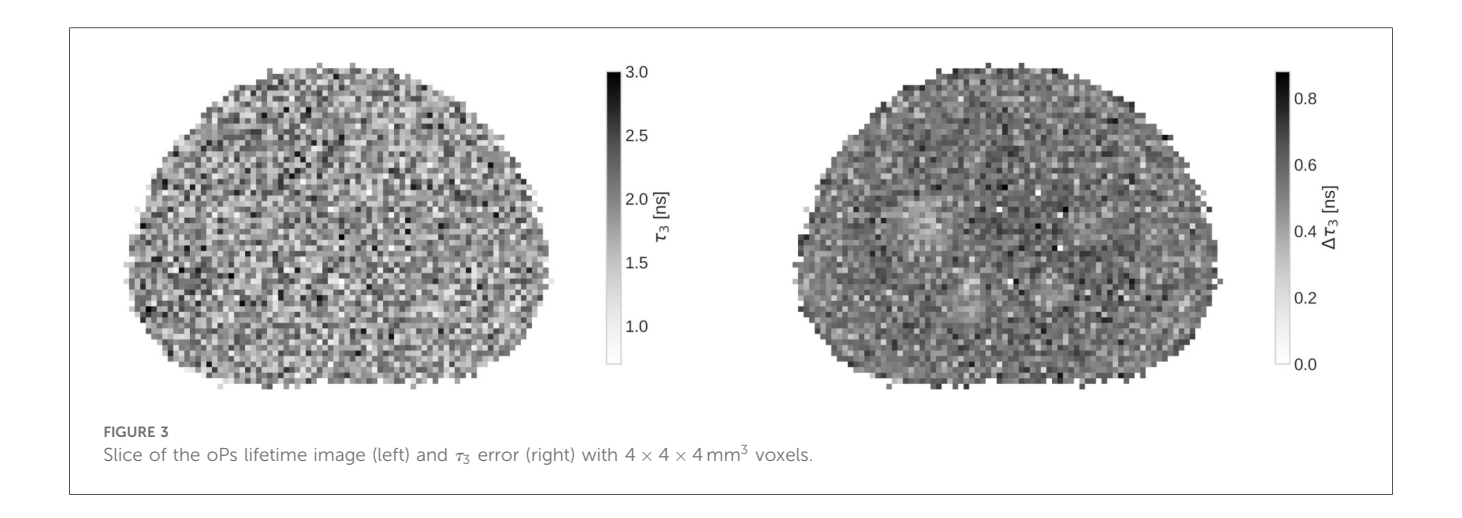
## 4 Discussion

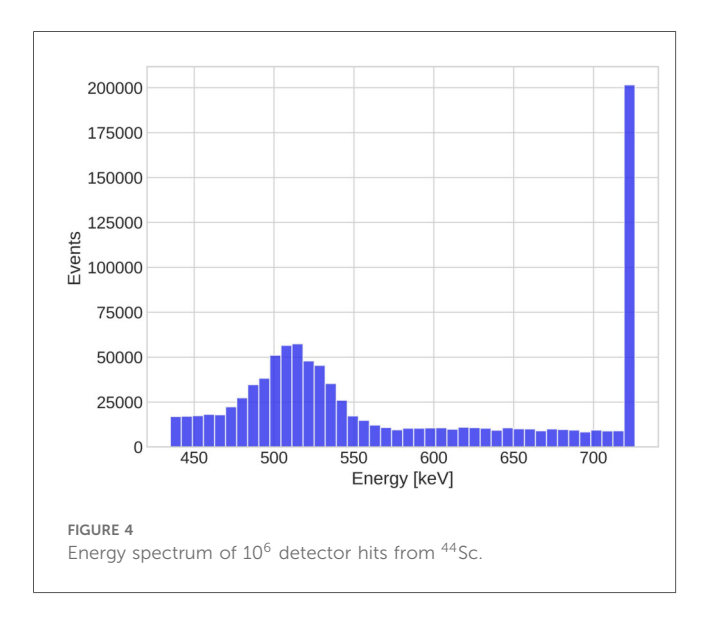
From the discussion in Ref. (34), it is clear that the key question is whether the high  $BR_{\gamma}$  of  $^{44}Sc$  can overcome the

Quadra's inability to resolve 44Sc's photopeak. Detector hits above 726 keV are collected in a single integrating bin, as clearly illustrated in Figure 4. One should, therefore, expect that more random coincidences are selected due to the high prompt-

TABLE 1 Fit results for the s	phantom spheres and	a single $4 \times 4 \times 4 \text{ mm}^3$	voxel in the center of $s_6$ .
-------------------------------	---------------------	---	--------------------------------

Fit	$ au_3$ [ns]	BR <sub>1</sub>	$HDI_{\mathit{BR}_1}$	BR <sub>2</sub>	$HDI_{\mathit{BR}_2}$	BR <sub>3</sub>	$HDI_{\mathit{BR}_3}$
<i>s</i> <sub>1</sub> ∅10 mm	$2.65 \pm 0.50$	0.072	[0.0, 0.091]	0.659	[0.608, 0.736]	0.269	[0.242, 0.301]
<i>s</i> <sub>2</sub> ∅13 mm	$1.39 \pm 0.20$	0.077	[0.049, 0.106]	0.623	[0.573, 0.679]	0.30	[0.267, 0.324]
s₃ Ø17 mm	$1.76 \pm 0.18$	0.062	[0.041, 0.083]	0.651	[0.62, 0.687]	0.287	[0.27, 0.301]
<i>s</i> <sub>4</sub> ∅22 mm	$1.86 \pm 0.09$	0.057	[0.047, 0.067]	0.655	[0.639, 0.671]	0.288	[0.281, 0.296]
<i>s</i> <sub>5</sub> ∅28 mm	$1.73 \pm 0.1$	0.091	[0.08, 0.103]	0.603	[0.585, 0.622]	0.306	[0.296, 0.314]
<i>s</i> <sub>6</sub> ∅37 mm	$1.78 \pm 0.08$	0.066	[0.057, 0.076]	0.642	[0.627, 0.657]	0.292	[0.285, 0.299]
Voxel	$1.79 \pm 0.57$	0.051	[0.0, 0.063]	0.609	[0.553, 0.717]	0.34	[0.266, 0.386]





photon energy of  $^{44}$ Sc. The right panel of Figure 3 already hints towards a high random  $3\gamma E$  rate: even inside the spheres, the relative error in the background region of the PAL spectrum exceeds 20%. For a comparison, Ref. (50) only considered those voxels with less than 20% background error for oPs lifetime imaging.

The large number of random  $3\gamma E$  is reflected in the statistical uncertainty of  $\tau_3$  reported in Table 1. All values for  $\tau_3$  in the phantom are consistent with the literature value of  $1.839 \pm 0.015$  ns for water from Ref. (54) and with the results from Ref. (50) within

their statistical uncertainty [note also the reference values in Ref. (17)]. However, the marginalized uncertainties reported in Table 1 are rather large: only starting from  $s_3$  the relative error starts dropping below 10% (and reaches even 31.9 % in a single voxel). This is likely more than the precision required to sense different oxygenation levels in lesions, as discussed in Ref. (16).

 $au_3$ 's uncertainty is seen in Figure 3 as well. The variation on  $au_3$  across the whole phantom is quite large, given that the expected oPs lifetime should be the same across the whole phantom. In the right panel of Figure 3, only very few voxels have an error below 0.3 ns. The mean uncertainty on  $au_3$  across the slice shown in Figure 3 is 0.53 ns. Only the four largest spheres of the phantom have a visibly smaller uncertainty compared to the phantom background.

The fit of the oPs lifetime critically depends on the time differences after the peak in the PAL spectrum, i.e., on values close to the random  $3\gamma E$  background. A useful quantity to characterize the  $3\gamma E$  count statistics is therefore the peak signal-to-background ratio (pSBR) in a PAL spectrum. In the measurements with  $^{124}I$ , Ref. (50) reported a pSBR of about 55.5 for a  $4\times4\times4$  mm³ voxel in the water tube with an activity concentration of  $252\,kBq/ml$  and a scan time of  $15\,min$ . For the PAL spectrum in the  $4\times4\times4$  mm³ voxel in Figure 2, however, the pSBR is only about 12.6. Despite the activity concentration being higher in the  $^{124}I$  measurements of Ref. (50), the scan duration is 5 min shorter. The error on  $\tau_3$  in a single voxel (last row in Table 1) is about four times larger than the error reported in Ref. (50) for the same voxel size. A similar picture arises when looking at volumes of similar size, e.g., the sphere  $s_4$ 

has a volume of 5.57 mL and is comparable with the volume of the tubes in Ref. (50). The relative error on  $\tau_3$ , however, is 4.8% while Ref. (50) reports a 1.1% error for a 5 mL tube with water. This comparison is even more striking, when considering the BR<sub>v</sub> per positron, which is almost 8 times higher for 44Sc than for <sup>124</sup>I. With the given methodology, resolving the photopeak therefore seems key for a low random  $3\gamma E$  rate. <sup>44</sup>Sc's high BR<sub> $\gamma$ </sub> cannot overcome Quadra's limited detection capabilities for high-energy photons. Given the energy spectrum in Figure 4, it is clear that extending the prompt-photon energy window does not yield a significant reduction of random 3 vE. Also, note that 124 I's lower prompt-photon energy (almost half compared to <sup>44</sup>Sc) increases the probability to interact within the detector crystals. It should be emphasized that this conclusion applies to the given methodology. Different detection methods (24) or event selection procedures and/or random 3yE estimations as e.g., in Ref. (55) may reduce the uncertainties on  $\tau_3$  in the case of high-energy prompt-photons. We leave such an investigation for future studies.

Ref. (56) did not attempt to perform a voxel-wise fit nor a fit to the three smallest spheres of the NEMA phantom. On the other hand, Ref. (57) seems to be able to fully exploit the high prompt-photon BR $_{\gamma}$  of <sup>44</sup>Sc. Both scanners in these studies do not suffer from the limited energy range of Quadra and the event selection and reconstruction algorithms are different.

In contrast to  $^{44}$ Sc,  $^{43}$ Sc's prompt photon is within Quadra's energy range and therefore, the afore mentioned discussion of the high-energy prompt-photons does not apply. However, the BR $_{\gamma}$  per positron is in the same order of magnitude as  $^{124}$ I and  $^{82}$ Rb i.e., much lower than for  $^{44}$ Sc.

#### 5 Conclusions

Given Quadra's limited energy resolution and the current methodology for selecting  $3\gamma E$ , it does not seem that  $^{44}Sc$  is able to outperform  $^{124}I$  in terms of count statistics for oPs lifetime imaging, despite its favorable physical properties and clinical prospects.

# Data availability statement

The raw data format is not publicly available. Evaluated data are available upon reasonable request. Requests to access the datasets should be directed to lorenzo.mercolli@insel.ch.

### **Author contributions**

LM: Writing – original draft, Investigation, Data curation, Writing – review & editing, Methodology, Conceptualization, Software, Funding acquisition, Formal analysis. WMS: Writing – review & editing, Software, Methodology, Investigation. PG: Resources, Investigation, Writing – review & editing. AM: Investigation, Resources, Writing – review & editing. SB:

Resources, Writing – review & editing. MC: Software, Writing – review & editing. PM: Writing – review & editing, Funding acquisition. NR: Writing – review & editing. AR: Writing – review & editing, Funding acquisition. HS: Writing – review & editing, Methodology, Software. RS: Writing – review & editing. RS: Writing – review & editing. KS: Funding acquisition, Writing – review & editing. ES: Funding acquisition, Writing – review & editing. NM: Funding acquisition, Writing – review & editing, Resources, Conceptualization.

# **Funding**

The author(s) declare that financial support was received for the research and/or publication of this article. This research is partially supported by the grant no. 216944 under the Weave/Lead Agency program of the Swiss National Science Foundation and the National Science Centre of Poland through grant OPUS24+LAP No. 2022/47/I/NZ7/03112 and 2021/43/B/ST2/02150. The dangerous good transportation was financed by the Research Fund of the Swiss Society of Radiobiology and Medical Physics.

# Conflict of interest

WMS and MC are full-time employees of Siemens Medical Solutions USA, Inc. HS is a part-time employee of Siemens Healthineers International AG. PM is an inventor on a patent related to this work. Patent nos.: (Poland) PL 227658, (Europe) EP 3039453, and (United States) US 9,851,456, filed (Poland) 30 August 2013, (Europe) 29 August 2014, and (United States) 29 August 2014; published (Poland) 23 January 2018, (Europe) 29 April 2020, and (United States) 26 December 2017. AR has received research support and speaker honoraria from Siemens. KS received research grants from Novartis and Siemens and conference sponsorships from United Imaging, Siemens, and Subtle Medical not related to the submitted work.

The remaining authors declare that the research was conducted in the absence of any commercial or financial relationships that could be construed as a potential conflict of interest

#### Generative Al statement

The author(s) declare that no Generative AI was used in the creation of this manuscript.

Any alternative text (alt text) provided alongside figures in this article has been generated by Frontiers with the support of artificial intelligence and reasonable efforts have been made to ensure accuracy, including review by the authors wherever possible. If you identify any issues, please contact us.

#### Publisher's note

All claims expressed in this article are solely those of the authors and do not necessarily represent those of their affiliated

organizations, or those of the publisher, the editors and the reviewers. Any product that may be evaluated in this article, or claim that may be made by its manufacturer, is not guaranteed or endorsed by the publisher.

### References

- 1. Čížek J. Characterization of lattice defects in metallic materials by positron annihilation spectroscopy: a review. *J Mater Sci Technol.* (2018) 34:577–98. doi: 10. 1016/j.jmst.2017.11.050
- 2. Gidley DW, Peng HG, Vallery RS. Positron annihilation as a method to characterize porous materials. *Annu Rev Mater Res.* (2006) 36:49–79. doi: 10.1146/annurev.matsci.36.111904.135144
- 3. Jean YC, Van Horn JD, Hung WS, Lee KR. Perspective of positron annihilation spectroscopy in polymers. *Macromolecules (Washington, DC, U. S.).* (2013) 46:7133–45. doi: 10.1021/ma401309x
- 4. Kobayashi Y, Ito K, Oka T, Hirata K. Positronium chemistry in porous materials. *Radiat Phys Chem.* (2007) 76:224–30. doi: 10.1016/j.radphyschem.2006.03.042
- 5. Schmidt W. Chap. 2.13: Positron annihilation spectroscopy. In: Schüth F, Sing KSW, Weitkamp J, editors. *Handbook of Porous Solids*. Weinheim: John Wiley & Sons, Ltd (2008). p. 506–32. doi: 10.1002/9783527618286.ch15
- 6. Schultz PJ, Lynn KG. Interaction of positron beams with surfaces, thin films, and interfaces. *Rev Mod Phys.* (1988) 60:701–79. doi: 10.1103/RevModPhys.60.701
- 7. Süvegh K, Marek T. Positron annihilation spectroscopies. In: Vértes A, Nagy S, Klencsár Z, Lovas RG, Rösch F, editors. *Handbook of Nuclear Chemistry*. Boston, MA: Springer US (2011). p. 1461–84. doi: 10.1007/978-1-4419-0720-2\_27
- 8. Tuomisto F, Makkonen I. Defect identification in semiconductors with positron annihilation: experiment and theory. *Rev Mod Phys.* (2013) 85:1583–631. doi: 10. 1103/RevModPhys.85.1583
- 9. Moskal P, Jasińska B, Stepień EŁ, Bass SD. Positronium in medicine and biology. Nat Rev Phys. (2019) 1:527–9. doi: 10.1038/s42254-019-0078-7
- 10. Bass SD, Mariazzi S, Moskal P, Stepień EŁ.. Colloquium: positronium physics and biomedical applications. *Rev Mod Phys.* (2023) 95:021002. doi: 10.1103/RevModPhys.95.021002
- 11. Hourlier A, Boisson F, Brasse D. Experimental uses of positronium and potential for biological applications. *IEEE Trans Radiat Plasma Med Sci.* (2024) 8:581–94. doi: 10.1109/TRPMS.2024.3407981
- 12. Moskal P, Bilewicz A, Das M, Huang B, Khreptak A, Parzych S, et al. Positronium imaging: history, current status, and future perspectives. In: *IEEE Transactions on Radiation and Plasma Medical Sciences* [Print]. arXiv:2503.14120 (2025).
- 13. Moskal P. Positronium imaging. In: 2019 IEEE Nuclear Science Symposium and Medical Imaging Conference (NSS/MIC) (2019). p. 1–3. doi: 10.1109/NSS/MIC42101. 2019.9059856
- 14. Axpe E, Lopez-Euba T, Castellanos-Rubio A, Merida D, Garcia JA, Plaza-Izurieta L, et al. Detection of atomic scale changes in the free volume void size of three-dimensional colorectal cancer cell culture using positron annihilation lifetime spectroscopy. *PLoS ONE*. (2014) 9:e83838. doi: 10.1371/journal.pone.0083838
- 15. Moskal P, Kisielewska D, Curceanu C, Czerwiński E, Dulski K, Gajos A, et al. Feasibility study of the positronium imaging with the J-PET tomograph. *Phys Med Biol.* (2019) 64:055017. doi: 10.1088/1361-6560/aafe20
- 16. Shibuya K, Saito H, Nishikido F, Takahashi M, Yamaya T. Oxygen sensing ability of positronium atom for tumor hypoxia imaging. *Commun Phys.* (2020) 3:173. doi: 10.1038/s42005-020-00440-z
- 17. Stepanov PS, Selim FA, Stepanov SV, Bokov AV, Ilyukhina OV, Duplâtre G, et al. Interaction of positronium with dissolved oxygen in liquids. *Phys Chem Chem Phys PCCP*. (2020) 22:5123–31. doi: 10.1039/C9CP06105C
- 18. Moskal P, Dulski K, Chug N, Curceanu C, Czerwiński E, Dadgar M, et al. Positronium imaging with the novel multiphoton PET scanner. Sci~Adv.~(2021) 7: eabh4394. doi: 10.1126/sciadv.abh4394
- 19. Moskal P, Stepień EŁ.. Positronium as a biomarker of hypoxia. *Bio-Algorithms Med-Syst.* (2021) 17:311–9. doi: 10.1515/bams-2021-0189
- 20. Qi J, Huang B. Positronium lifetime image reconstruction for TOF PET. *IEEE Trans Med Imaging.* (2022) 41:2848–55. doi: 10.1109/TMI.2022.3174561
- 21. Moskal P, Kubicz E, Grudzień G, Czerwiński E, Dulski K, Leszczyński B, et al. Developing a novel positronium biomarker for cardiac myxoma imaging. *EJNMMI Phys.* (2023) 10:22. doi: 10.1186/s40658-023-00543-w
- 22. Chen Z, An L, Kao CM, Huang HH. The properties of the positronium lifetime image reconstruction based on maximum likelihood estimation. *Bio-Algorithms Med-Syst.* (2023) 19:1–8. doi: 10.5604/01.3001.0054.1807

- 23. Takyu S, Matsumoto K, Hirade T, Nishikido F, Akamatsu G, Tashima H, et al. Quantification of radicals in aqueous solution by positronium lifetime: an experiment using a clinical PET scanner. *Jpn J Appl Phys.* (2024) 63:086003. doi: 10.35848/1347-4065/ad679a
- 24. Moskal P, Baran J, Bass S, Choiński J, Chug N, Curceanu C, et al. Positronium image of the human brain in vivo. Sci~Adv.~(2024)~10:eadp2840. doi: 10.1126/sciadv. adp2840
- 25. Mercolli L, Steinberger WM, Sari H, Afshar-Oromieh A, Caobelli F, Conti M, et al. In vivo positronium lifetime measurements with a long axial field-of-view PET/CT. *medRxiv.* (2024). doi: 10.1101/2024.10.19.24315509
- 26. Mercolli L, Steinberger WM, Läppchen T, Amon M, Bregenzer C, Conti M, et al. In vivo intralesional positronium lifetime imaging of thyroid cancer using clinically routine i-124 pet/ct. *medRxiv*. (2025). doi: 10.1101/2025.05.28.25328504
- 27. Shopa RY, Dulski K. Positronium imaging in J-PET with an iterative activity reconstruction and a multi-stage fitting algorithm. *Bio-Algorithms Med-Syst.* (2023) 19:54–63. doi: 10.5604/01.3001.0054.1826
- 28. Huang B, Qi J. High-resolution positronium lifetime tomography by the method of moments. *Phys Med Biol.* (2024) 69:24NT01. doi: 10.1088/1361-6560/ad9543
- 29. Chen Z, Kao CM, Huang HH, An L. Enhanced positronium lifetime imaging through two-component reconstruction in time-of-flight positron emission tomography. *Front Phys.* (2024) 12:1429344. doi: 10.3389/fphy.2024.1429344
- 30. Berens L, Hsu I, Chen CT, Halpern H, Kao CM. An analytic, moment-based method to estimate orthopositronium lifetimes in positron annihilation lifetime spectroscopy measurements. *Bio-Algorithms Med-Syst.* (2024) 20:40–8. doi: 10.5604/01.3001.0054.9141
- 31. Huang B, Wang Z, Zeng X, Goldan A, Qi J. Fast high-resolution lifetime image reconstruction for positron lifetime tomography. Commun Phys. (2025) 8:181. doi: 10.1038/s42005-025-02100-6
- 32. H-H Huang HH, Zhu Z, Booppasiri S, Chen Z, Pang S, Kao CM. A statistical reconstruction algorithm for positronium lifetime imaging using time-of-flight positron emission tomography. *IEEE Trans Radiat Plasma Med Sci.* (2025) 9:478–86. doi: 10.1109/TRPMS.2025.3531225
- 33. Moskal P, Kisielewska D, Shopa R, Bura Z, Chhokar J, Curceanu C, et al. Performance assessment of the 2gamma positronium imaging with the total-body PET scanners. *EJNMMI Phys.* (2020) 7:44. doi: 10.1186/s40658-020-00307-w
- 34. Steinberger WM, Mercolli L, Breuer J, Sari H, Parzych S, Niedzwiecki S, et al. Positronium lifetime validation measurements using a long-axial field-of-view positron emission tomography scanner. *EJNMMI Phys.* (2024) 11:76. doi: 10.1186/s40658-024-00678-4
- 35. Alberts I, Hünermund JN, Prenosil G, Mingels C, Bohn KP, Viscione M, et al. Clinical performance of long axial field of view PET/CT: a head-to-head intra-individual comparison of the Biograph Vision Quadra with the Biograph Vision PET/CT. Eur J Nucl Med Mol Imaging. (2021) 48:2395–404. doi: 10.1007/s00259-021-05282-7
- 36. Prenosil GA, Sari H, Fürstner M, Afshar-Oromieh A, Shi K, Rominger A, et al. Performance characteristics of the Biograph Vision Quadra PET/CT system with a long axial field of view using the NEMA NU 2-2018 standard. *J Nucl Med.* (2022) 63:476–84. doi: 10.2967/jnumed.121.261972
- 37. Spencer BA, Berg E, Schmall JP, Omidvari N, Leung EK, Abdelhafez YG, et al. Performance evaluation of the uEXPLORER total-body PET/CT scanner based on NEMA NU 2-2018 with additional tests to characterize PET scanners with a long axial field of view. *J Nucl Med.* (2021) 62:861–70. doi: 10.2967/jnumed.120.250597
- 38. Moskal P, Stepien E. Prospects and clinical perspectives of total-body PET imaging using plastic scintillators. *PET Clin.* (2020) 15:439–52. doi: 10.1016/j.cpet. 2020.06.009
- 39. Das M, Mryka W, Beyene EY, Parzych S, Sharma S, Stepień EŁ, et al. Estimating the efficiency and purityfor detecting annihilation and promptphotons for positronium imagingwith j-pet using toy monte carlosimulation. *Bio-Algorithms Med-Syst.* (2023) 19:87–95. doi: 10.5604/01.3001.0054.1938
- 40. Müller C, Bunka M, Haller S, Köster U, Groehn V, Bernhardt P, et al. Promising prospects for 44Sc-/47Sc-based theragnostics: application of 47Sc for radionuclide tumor therapy in mice. *J Nucl Med.* (2014) 55:1658–64. doi: 10.2967/jnumed.114. 141614

- 41. Singh A, Baum R, Klette I, van der Meulen N, Mueller C, Tuerler A, et al. Scandium-44 DOTATOC PET/CT: First in-human molecular imaging of neuroendocrine tumors and possible perspectives for Theranostics. *J Nucl Med.* (2015) 56:267–. doi: 10.2967/jnumed.115.160366
- 42. Eppard E, de la Fuente A, Benešová M, Khawar A, Bundschuh RA, Gärtner FC, et al. Clinical translation and first in-human use of [44Sc]Sc-PSMA-617 for PET imaging of metastasized castrate-resistant prostate cancer. *Theranostics*. (2017) 7:4359–69. doi: 10.7150/thno.20586
- 43. Umbricht CA, Benešová M, Schmid RM, Türler A, Schibli R, van der Meulen NP, et al. 44Sc-PSMA-617 for radiotheragnostics in tandem with 177Lu-PSMA-617-preclinical investigations in comparison with 68Ga-PSMA-11 and 68Ga-PSMA-617. *EJNMMI Res.* (2017) 7:9. doi: 10.1186/s13550-017-0257-4
- 44. Müller C, Domnanich KA, Umbricht CA, van der Meulen NP. Scandium and terbium radionuclides for radiotheranostics: current state of development towards clinical application. *Br J Radiol.* (2018) 91:20180074. doi: 10.1259/bjr. 20180074
- 45. Zhang J, Singh A, Kulkarni HR, Schuchardt C, Müller D, Wester HJ, et al. From bench to bedside—the bad berka experience with first-in-human studies. *Semin Nucl Med.* (2019) 49:422–37. doi: 10.1053/j.semnuclmed.2019.06.002. From Basic Science to Clinical Imaging
- 46. van der Meulen NP, Hasler R, Talip Z, Grundler PV, Favaretto C, Umbricht CA, et al. Developments toward the implementation of 44Sc production at a medical cyclotron. *Molecules*. (2020) 25:4706. doi: 10.3390/molecules25204706
- 47. Lima T, Gnesin S, Nitzsche E, Ortega P, Müller C, van der Meulen N. First phantom-based quantitative assessment of scandium-44 using a commercial PET device. *Front Phys.* (2020) 8:241. doi: 10.3389/fphy.2020.00241
- 48. Lima TVM, Gnesin S, Strobel K, Pérez MS, Roos JE, Müller C, et al. Fifty shades of scandium: comparative study of PET capabilities using Sc-43 and Sc-44 with respect to conventional clinical radionuclides. *Diagnostics*. (2021) 11:1826. doi: 10. 3390/diagnostics11101826

- 49. van der Meulen NP, Strobel K, Lima TVM. New radionuclides and technological advances in SPECT and PET scanners. *Cancers.* (2021) 13:6183. doi: 10.3390/cancers13246183
- 50. Mercolli L, Steinberger WM, Rathod N, Conti M, Moskal P, Rominger A, et al. Phantom imaging demonstration of positronium lifetime with a long axial field-of-view PET/CT and (124)I. *EJNMMI Phys.* (2025) 12:80. doi: 10.1186/s40658-025-00790-z
- 51. Grundler PV, Eichler R, Talip Z, Schubiger PA, Schibli R, van der Meulen NP. The metamorphosis of radionuclide production and development at Paul Scherrer Institute. *CHIMIA*. (2020) 74:968. doi: 10.2533/chimia.2020.968
- 52. Braccini S, Belver-Aguilar C, Carzaniga T, Dellepiane G, Haeffner P, Scampoli P. Novel irradiation methods for theranostic radioisotope production with solid targets at the bern medical cyclotron. In: 22nd International Conference on Cyclotrons and their Applications (CYC2019) (2020). p. TUA02. doi: 10.18429/JACoW-Cyclotrons2019-TUA02
- 53. Juget F, Durán T, Nedjadi Y, Talip Z, Grundler PV, Favaretto C, et al. Activity measurement of 44Sc and calibration of activity measurement instruments on production sites and clinics. *Molecules*. (2023) 28:1345. doi: 10.3390/molecules28031345
- $54.~{\rm Kotera}$  K, Saito T, Yamanaka T. Measurement of positron lifetime to probe the mixed molecular states of liquid water. *Phys Lett A.* (2005) 345:184–90. doi: 10.1016/j. physleta.2005.07.018
- 55. Huang B, Li T, Arino-Estrada G, Dulski K, Shopa RY, Moskal P, et al. SPLIT: statistical positronium lifetime image reconstruction via time-thresholding. *IEEE Trans Med Imaging*. (2024) 43:2148–58. doi: 10.1109/TMI.2024.3357659
- 56. Das M, Sharma S, Beyene EY, Bilewicz A, Choinski J, Chug N, et al. First positronium imaging using 44Sc with the J-PET scanner: a case study on the NEMA-image quality phantom. *IEEE Trans Radiat Plasma Med Sci.* (2025):1. doi: 10.1109/TRPMS.2025.3621554
- 57. Huang B, Dai B, Lapi SE, Liles G, Karp JS, Qi J. High-resolution positronium lifetime tomography at clinical activity levels on the PennPET explorer. *J Nucl Med.* (2025) 66:1464–70. doi: 10.2967/jnumed.125.270130